Tuning the Growth Orientation of Epitaxial Films by Interface Chemistry

Matthias Gubo, Christina Ebensperger, Wolfgang Meyer, Lutz Hammer, and Klaus Heinz
Lehrstuhl für Festkörperphysik, Universität Erlangen-Nürnberg, Staudtstraße 7, D-91058 Erlangen, Germany

Florian Mittendorfer* and Josef Redinger
Institut für Angewandte Physik and Center for Computational Materials Science, Technische Universität Wien, Gußhausstraße 25/134, A-1040 Wien, Austria

(Received 24 October 2011; published 10 February 2012)

The support of epitaxial films frequently determines their crystallographic orientation, which is of crucial importance for their properties. We report a novel way to alter the film orientation without changing the substrate. We show for the growth of CoO on the Ir(100) surface that, while the oxide grows in (111) orientation on the bare substrate, the orientation switches to (100) by introducing a single (or a few) monolayer(s) of Co between the oxide and substrate. This tunability of the orientation of epitaxial films by the appropriate choice of interface chemistry most likely is a general feature.

DOI: 10.1103/PhysRevLett.108.066101 PACS numbers: 68.35.Ct, 68.47.Gh, 68.55.Nq, 68.90.+g

Epitaxial films of transition-metal oxides grown on metal surfaces have been intensely investigated recently (for a review, see Ref. [1]). On most (100) oriented substrates with face-centered-cubic symmetry, the rocksalt-structured oxide films grow in the low-indexed (100) or (111) orientation. It is often argued that the size of the lattice misfit between the oxide and support—mirrored by the (compressive) strain ϵ under which (100) oriented oxides would suffer in pseudomorphic film growth—is decisive for the film orientation, which in turn is crucial for their physical properties. Indeed, for small strain values (100) oriented oxides were observed for NiO [2] and CoO [3] on Ag(100) ($\epsilon = 2.0\%$ and 4.1%, respectively), while for large strain as for CoO/Ir(100) [4–8] and MnO/Rh(100) [9] ($\epsilon = 9.9\%$ and 14.5%, respectively) films in (111) orientation develop. Yet, in a number of cases (100) films were observed with even considerable nominal strain involved, for example, on Pd(100) for NiO [10–12] ($\epsilon = 6.7\%$), CoO [13,14] ($\epsilon = 8.7\%$), or MnO [15–17] ($\epsilon = 12.5\%$). In these cases, however, the (100)-type growth starts with a layer exhibiting a $c(4 \times 2)$ periodic near rhombic arrangement of transition-metal vacancies, equivalent to overall TM_4O_3 stoichiometry, which is supposed to allow for strain relief.

In contrast, for CoO/Ir(100)—for which the nominal strain ($\epsilon = 9.9\%$) fits to the range of the above cases—no Co_3O_4/Ir(100) phase is observed. This indicates that the oxide's orientation is dominated by the chemical interaction between the film and substrate rather than by strain. This is illustrated by showing that for CoO on Ir the growth can be switched from (111) orientation on the bare substrate to (100) when one or a few (m) pseudomorphic Co monolayers (ML) are introduced as an additional interface between the oxide and support *whereby the oxide's strain remains the same*. In the initial oxidation process, this leads to Co_3O_4/m ML Co/Ir(100) phases whereby the oxide exhibits the same $c(4 \times 2)$ superstructure of Co vacancies as cited. By further deposition and oxidation of Co, vacancy-free CoO(100) layers grow whose lattice parameter relaxes towards that of bulk CoO.

We apply both experimental and theoretical methods, i.e., quantitative low-energy electron diffraction (LEED) and scanning tunneling microscopy (STM) as well as first-principles calculations based on density functional theory (DFT). The calculations not only confirm the structural results obtained by the LEED analysis but also show that the $Co_3O_4 - c(4 \times 2)$ phase is unstable on the bare Ir(100) surface but can be stabilized on 1 ML Co/Ir(100). For the present epitaxial system, we prove that the mere consideration of strain and stress is too simple and that the chemistry of the very interface is crucial, as it tunes the oxide's orientation whereby the $c(4 \times 2)$ phase is a precursor for (100) growth.

The initial oxide grown on the unreconstructed Ir(100) $-$ (1×1) surface was prepared by deposition of several pseudomorphic Co monolayers in the range $1\frac{3}{4}$–$5\frac{3}{4}$ ML (i.e., with an incomplete top layer of about $\frac{3}{4}$ ML coverage in order to eventually achieve a film of uniform height). They were exposed to an oxygen atmosphere (5×10^{-9} mbar) for about 1 min at 320 K followed by annealing at 670 K. Independent of the number m of full Co layers, a well-ordered $c(4 \times 2)$ superstructure develops which, as will be shown, is confined to the top layer and exhibits a $c(4 \times 2)$ periodic arrangement of Co vacancies. The $c(4 \times 2) - Co_3O_4/m$ ML Co/Ir(100) phases and the further growth of (100) oriented CoO were investigated by LEED and STM for $m = 1$–5 (for $m = 0$ these phases do not develop). The structure and energetics of a single $c(4 \times 2)$ oxide layer—which is a crucial precursor for (100) film growth—were investigated by quantitative LEED (for $m = 1$ and 3) and DFT (for $m = 1$). The LEED intensities were recorded at normal incidence and for the sample at 100 K by using a computer-controlled video

method [18]. They were evaluated by applying the perturbation method TENSORLEED [18,19] by use of the TENSERLEED code [20]. A structural search procedure [21] was applied controlled by the Pendry R factor R [22]. DFT calculations were performed with the Vienna *ab initio* simulation package (VASP) [23], by using projector augmented wave potentials [24] and the Perdew-Burke-Ernzerhof exchange-correlation functional [25]. A k-mesh grid of $16 \times 16 \times 1$ points in the (1×1) cell was used for the Brillouin zone integration. As the DFT calculations do not capture the full correlation effects of bulk CoO, both standard DFT and density-functional theory plus Coulomb repulsion parameter U (DFT + U) [26] values are reported ($U - J = 1$). The substrate was modeled by a five-layer slab, where the two uppermost layers were allowed to relax. The surface stress was evaluated from an explicit deformation of the supercell [27,28]. The phase diagrams have been constructed in the framework of the *ab initio thermodynamics* [29].

In the initial preparation procedure, only the (incomplete) top Co layer is oxidized. Figures 1(a) and 1(b) display the LEED and STM images for $m = 1$ (i.e., a $\frac{3}{4}$ ML Co on top of a full Co layer). The inset in the latter shows that the $c(4 \times 2)$ structure is due to deep depressions, each surrounded by 8 protrusions. By further exposure of a $c(4 \times 2) - Co_3O_4/m$ ML Co/Ir(100) phase with several monolayers of Co to oxygen at first small CoO(100) islands develop as displayed in Fig. 1(d) for $m = 5$. Below them, the $c(4 \times 2)$ phase is transformed to CoO(100) forming a moiré structure of about (12×12) periodicity [Fig. 1(c)]. It stems from the superposition of the more or less unstrained CoO(100) and the substrate. The $c(4 \times 2)$ spots have disappeared. In the hollow-type areas of the moiré structure, there are again CoO(100) islands [Fig. 1(e)]. Their size (≈ 20 Å) seems to be limited by that of the moiré hollows, and their spacing is according to the superstructure periodicity, i.e., $12a_{p,\mathrm{Ir}} \approx 33$ Å ($a_{p,\mathrm{Ir}} = 2.715$ Å). These results show that the $c(4 \times 2)$ phase is a precursor for the growth of CoO(100). Indeed, further film growth by reactive deposition of Co leads to a fourfold symmetric LEED pattern and a STM image with quadratically arranged protrusions [Figs. 1(f) and 1(g)], both consistent with the bulk lattice parameter of CoO. Similar to the (111) films growing on bare Ir [see the LEED and STM images in Figs. 1(h) and 1(i)] and being stable up to high temperatures [4–8], the (100) films are stable up to 1000 °C.

As the $c(4 \times 2)$ phase plays a crucial role as a precursor for (100) growth and develops only on the additional Co interface but not on the bare substrate, it deserves a detailed investigation of its structure, energetics, and stability. By LEED intensity analysis we retrieve a vacancy model similar to that found for $c(4 \times 2) - Ni_3O_4/Pd(100)$ [10,11]. Yet, in contrast to the latter, a convincing agreement of experimental and calculated spectra ($R = 0.172$) can be achieved only with the additional Co layer below the oxide. Also, in-plane and vertical relaxations induced by the vacancies are essential. Figure 2 displays the best-fit model in top (a) and side views [(b) and (c)], whereby

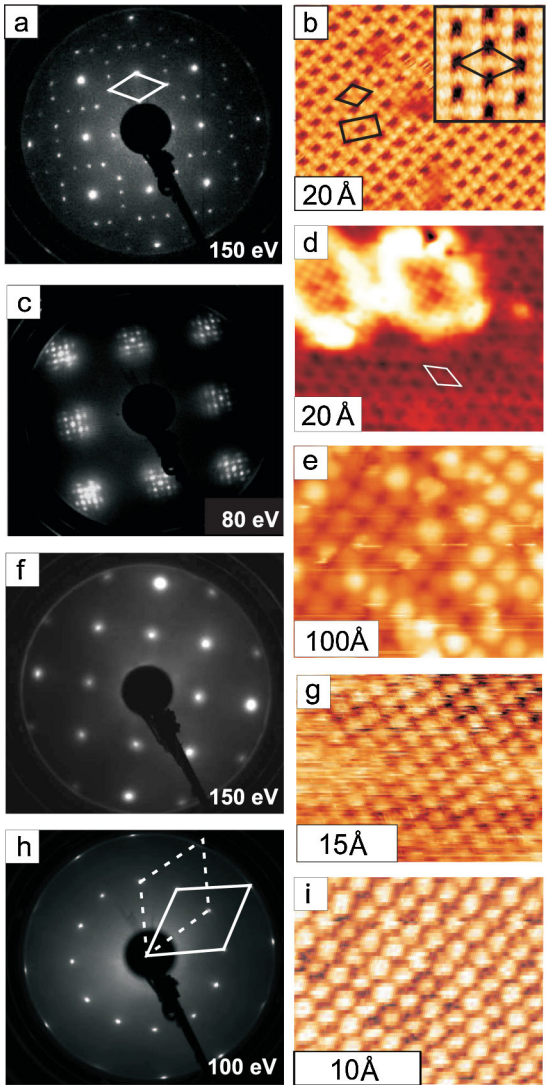

FIG. 1 (color online). LEED pattern (a) and STM image (b) for $c(4 \times 2)Co_3O_4/1$ ML Co/Ir(100). The reciprocal unit cell is inserted in (a) and the centered and noncentered real space unit cells in (b). Panel (c) displays the LEED pattern resulting when a $c(4 \times 2)Co_3O_4/5$ ML Co/Ir(100) phase is further oxidized; panels (d) and (e) display corresponding STM images at different scales and oxidation states. In (f) and (g), the LEED pattern and STM image are given which develop for further reactive deposition of Co, i.e., growth of CoO(100). For comparison, the LEED pattern and STM image for a (111) oriented film growing on the bare Ir substrate are displayed in panels (h) and (i), respectively [6]. Note that there are 2 orthogonal domains.

panel (a) indicates two (reasonably assumed) mirror planes and the directions of in-plane shifts. In panels (b) and (c), the best-fit structural parameters are given. The values in brackets refer to the result from the DFT calculations, which are not significantly changed on the DFT + U level (< 0.01 Å). The deviations between LEED and DFT are not larger than 0.03 Å for the vertical bucklings and up to 0.07 Å for in-plane shifts with both values being of the order of accuracy applying to the two methods. The spectra for $Co_3O_4/3$ ML Co/Ir(100) were also analyzed

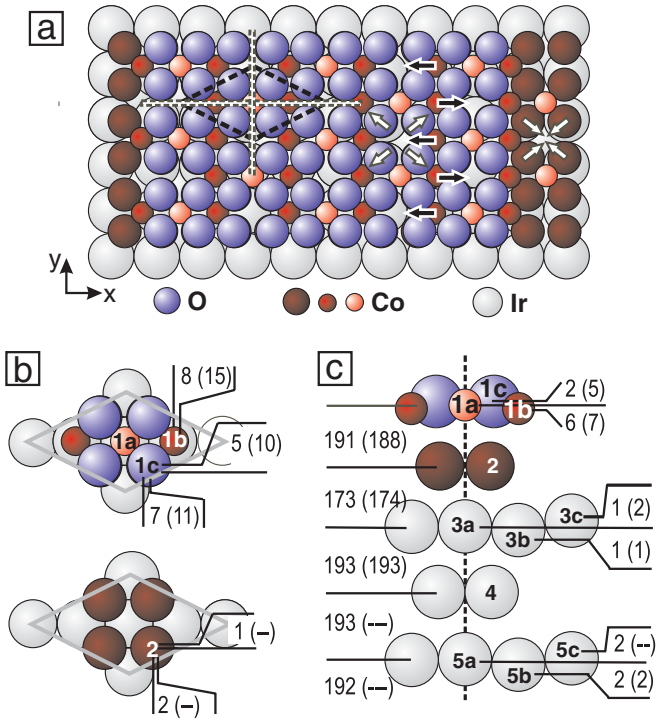

FIG. 2 (color online). Structure of Co_3O_4/1 ML Co/Ir(100) in top and side view. The arrows in (a) indicate the in-plane relaxations whose best-fit values are displayed in (b) denoting the shifts off the ideal hollow or top sites (lateral shifts in Ir layers turn out to be negligible). Vertical bucklings are given in (c); the layer spacings on the left are for the center of mass planes. All numbers refer to pm units; those in brackets correspond to the result of DFT.

($R = 0.174$), whereby the best-fit parameters of the oxide layer are close to those for $m = 1$.

Finally, we investigated the energetics of the films to elucidate the driving mechanism for the formation of the Co_3O_4 layer. The stability of the surface oxide layer is commonly related to the mismatch-induced strain. Yet, this is not a safe guide as several (100)-type surface oxide layers with a formally large lattice mismatch are experimentally observed as cited above. One of the reasons for this discrepancy is the reference value of the oxide's lattice parameter for which usually the bulk value is used. Yet, the low dimensionality of an *unsupported* oxide monolayer leads to a lattice compression. So, the DFT (DFT + U) calculations predict a lattice parameter of 4.22 Å (4.26 Å) for bulk CoO but 3.94 Å (3.94 Å) for a stoichiometric CoO single layer and even 3.75 Å (3.80 Å) for the Co_3O_4 layer. Although the interaction with the substrate will lead to a lattice expansion in comparison with the unsupported layer, these values still illustrate that the formal mismatch to the Ir lattice constant (3.88 Å) is significantly lower than commonly assumed.

Even more important is the stress in layers residing on the substrate. Although epitaxial growth leads to the same strain in the CoO layer on Ir(100) and CoIr(100), the interaction with the substrate leads to a difference in the surface stress. DFT (DFT + U) calculations predict only small stress values for Co_3O_4/Ir(100), i.e., $\tau_x = +0.033$ (-0.063) eV/Å^2 and $\tau_y = +0.009$ (-0.042) eV/Å^2. For Co_3O_4/Co/Ir(100), however, an *increase* of the surface stress results, i.e., $\tau_x = +0.354$ ($+0.126$) eV/Å^2 and $\tau_y = +0.289$ ($+0.144$) eV/Å^2. As a consequence, the stabilization of the Co_3O_4 layer by the additional interfacial Co layer is not driven by a reduction of surface stress.

Obviously, the films' stability is determined by the interplay of contributions from the film, the interface, and the substrate. Their sum is captured in the phase diagrams in Fig. 3. In this overview of the thermodynamic stability, the (100)-type $c(4 \times 2)$ phase and phases of slightly lower, $c(10 \times 2)$, and slightly higher, $c(8 \times 2)$, oxygen content are compared. Both phases have been found on the bare Ir substrate and correspond to a buckled Co-O(111) bilayer and a O-Co-O(111) trilayer [4,8,30]. Panel (a) displays the energetics of the phases on bare Ir and panel (b) that when interfaced by an additional Co layer, both as a function of the oxygen chemical potential. On the bare substrate, the $c(4 \times 2)$ is never the energetically favorable phase. The similar slope of the curves for the $c(4 \times 2)$ and $c(10 \times 2)$ phases is a result of the small difference in the oxygen content (1.0 vs 0.9 ML). In contrast, the situation changes completely with a Co layer at the interface between the oxide and substrate: The $c(4 \times 2)$ phase now is

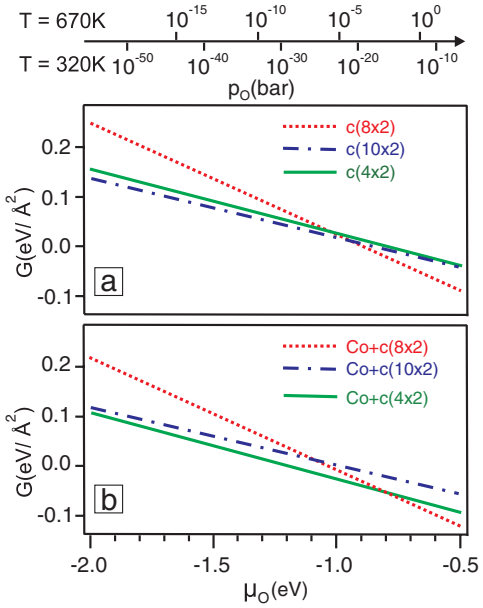

FIG. 3 (color online). Phase diagram for a single cobalt-oxide layer on (a) the bare Ir surface and (b) on 1 ML Co/Ir. G is the surface free energy, μ_O the chemical potential of oxygen, and p_O the corresponding oxygen pressure at the temperature of sample preparation, 320 and 670 K. The scale for p_O was calculated by using the relation $\ln(p_O/p_O^0) = (2/kT)(\mu_O - \mu_O^0)$ [31] with $p_O^0 = 1$ atm $= 981$ mbar (k is the Boltzmann constant). The zero point for the chemical potential is taken by interpolation from the list given in Ref. [31] resulting in $\mu_O^0 = -0.29$ eV for 320 K and $\mu_O^0 = -0.68$ eV for 670 K.

energetically favored in the experimentally relevant pressure and temperature range [panel (b)]. The reason for the higher stability of the CoO layer is directly related to the interface chemistry, as the Co interface layer significantly raises the interaction energy of the Co_3O_4 layer with the substrate from a value of -3.7 eV/unit cell for Ir(100) to -5.4 eV/unit cell for Co/Ir(100) (this is much less pronounced for the other phases). The stronger binding is also reflected by the oxygen-substrate bond length, which decreases from 2.15 Å on bare Ir(100) to 1.93 Å in the presence of interfacial Co, i.e., significantly more than caused by the different radii of Ir and Co. The binding scenario also explains why the $c(4 \times 2)$ phase does not develop without interfacial Co layers. The strong interaction of O with the interfacial Co is particularly important for the Co_3O_4 phase, which binds to the substrate exclusively via oxygen in a rocksalt configuration. This is different for the competing $c(8 \times 2)$ and $c(10 \times 2)$ phases, which both display a wide variety of bond configurations to the substrate.

In conclusion, we have demonstrated that the interface chemistry (and not the surface strain and stress) is crucial for the crystallographic orientation of CoO films epitaxially grown on Ir(100). In particular, the film orientation can be changed without changing the substrate. Important for the growth in (100) orientation is the development of a precursor state, i.e., a CoO(100)-type layer with $c(4 \times 2)$ periodic Co vacancies. This can be created on Ir(100) only when interfacing Co layers exist. The $c(4 \times 2)$ precursor state seems to be prototypical for (100) growth as it has been observed also for other oxides on other substrates. As we have shown, its formation is not driven by a reduction of surface stress, as the latter is lower for a (hypothetical) Co_3O_4/Ir(100) than for Co_3O_4/Co/Ir(100). Instead, the binding of the oxide to the support is important, whereby the chemical nature of the outermost atoms seems to be decisive. So, for the present system, there is a competition between monolayer phases of (111)- and (100)-type [the latter is the defective $c(4 \times 2)$ phase] which trigger (111) or (100) growth, respectively. The presence of interfacial Co layers favors (100) growth as if a chemically different substrate like, e.g., Pd were used. We therefore speculate that this chemical stabilization of a precursor phase can be a general phenomenon and that, consequently, the proper choice of the chemical interface between the film and support may be used to tune the growth orientation also in other systems.

The authors are grateful for financial support by the Deutsche Forschungsgemeinschaft (DFG) and the Austrian Science Fund (FWF) F4511-N16 and for the computer support of the Vienna Scientific Cluster (VSC).

*fmi@cms.tuwien.ac.at

[1] F. P. Netzer, F. Allegretti, and S. Surnev, J. Vac. Sci. Technol. B **28**, 1 (2010).
[2] A. Rota, S. Altieri, and S. Valeri, Phys. Rev. B **79**, 161401 (R) (2009).
[3] P. Torelli, E. A. Soares, G. Renaud, S. Valeri, X. X. Guao, and P. Luches, Surf. Sci. **601**, 2651 (2007).
[4] C. Giovanardi, L. Hammer, and K. Heinz, Phys. Rev. B **74**, 125429 (2006).
[5] W. Meyer, K. Biedermann, M. Gubo, L. Hammer, and K. Heinz, J. Phys. Condens. Matter **20**, 265011 (2008).
[6] W. Meyer, D. Hock, K. Biedermann, M. Gubo, S. Müller, L. Hammer, and K. Heinz, Phys. Rev. Lett. **101**, 016103 (2008).
[7] K. Biedermann, M. Gubo, L. Hammer, and K. Heinz, J. Phys. Condens. Matter **21**, 185003 (2009).
[8] C. Ebensperger, M. Gubo, W. Meyer, L. Hammer, and K. Heinz, Phys. Rev. B **81**, 235405 (2010).
[9] H. Nishimura, T. Tashiro, T. Fujitani, and J. Nakamura, J. Vac. Sci. Technol. A **18**, 1460 (2000).
[10] S. Agnoli, M. Sambi, G. Granozzi, A. Atrei, M. Caffio, and G. Rovida, Surf. Sci. **576**, 1 (2005).
[11] S. Agnoli, M. Sambi, G. Granozzi, J. Schoiswohl, S. Surnev, F. P. Netzer, M. Ferrero, A. M. Ferrari, and C. Pisani, J. Chem. Phys. **109**, 17 197 (2005).
[12] A. M. Ferrari, M. Ferrero, and C. Pisani, J. Phys. Chem. B **110**, 7918 (2006).
[13] L. Gragnaniello, S. Agnoli, G. Parteder, A. Barolo, F. Bondino, F. Allegretti, S. Surnev, and F. P. Netzer, Surf. Sci. **604**, 2002 (2010).
[14] F. Allegretti, G. Parteder, L. Gragnaniello, S. Surnev, F. P. Netzer, A. Barolo, S. Agnoli, G. Granozzi, C. Franchini, and R. Podloucky, Surf. Sci. **604**, 529 (2010).
[15] F. Li, G. Parteder, F. Allegretti, C. Franchini, R. Podloucky, S. Surnev, and F. P. Netzer, J. Phys. Condens. Matter **21**, 134008 (2009).
[16] C. Franchini, R. Podloucky, F. Allegretti, F. Li, G. Parteder, S. Surnev, and F. P. Netzer, Phys. Rev. B **79**, 035420 (2009).
[17] C. Franchini, J. Zabloudil, R. Podloucky, F. Allegretti, F. Li, S. Surnev, and F. P. Netzer, J. Chem. Phys. **130**, 124707 (2009).
[18] K. Heinz, Rep. Prog. Phys. **58**, 637 (1995).
[19] P. J. Rous, J. B. Pendry, D. K. Saldin, K. Heinz, K. Müller, and N. Bickel, Phys. Rev. Lett. **57**, 2951 (1986).
[20] V. Blum and K. Heinz, Comput. Phys. Commun. **134**, 392 (2001).
[21] M. Kottcke and K. Heinz, Surf. Sci. **376**, 352 (1997).
[22] J. B. Pendry, J. Phys. C **13**, 937 (1980).
[23] G. Kresse and J. Furthmüller, Phys. Rev. B **54**, 11 169 (1996); Comput. Mater. Sci. **6**, 15 (1996).
[24] G. Kresse and D. Joubert, Phys. Rev. B **59**, 1758 (1999).
[25] J. P. Perdew, K. Burke, and M. Ernzerhof, Phys. Rev. Lett. **77**, 3865 (1996).
[26] S. L. Dudarev, G. A. Botton, S. Y. Savrasov, C. J. Humphreys, and A. P. Sutton, Phys. Rev. B **57**, 1505 (1998).
[27] R. Westerström, C. J. Weststrate, A. Resta, A. Mikkelsen, J. Schnadt, J. N. Andersen, E. Lundgren, M. Schmid, N. Seriani, J. Harl, F. Mittendorfer, and G. Kresse, Surf. Sci. **602**, 2440 (2008).
[28] J. Harl, and G. Kresse, Surf. Sci. **600**, 4633 (2006).
[29] F. Mittendorfer, N. Seriani, O. Dubay, and G. Kresse, Phys. Rev. B **76**, 233413 (2007).
[30] M. Gubo, C. Ebensperger, W. Meyer, L. Hammer, and K. Heinz, Phys. Rev. B **83**, 075435 (2011).
[31] K. Reuter and M. Scheffler, Phys. Rev. B **65**, 035406 (2001).